Computers and Concrete, *Vol. 20, No. 5 (2017) 595-603*
DOI: https://doi.org/10.12989/cac.2017.20.5.595

Structural health monitoring using piezoceramic transducers as strain gauges and acoustic emission sensors simultaneously

Linsheng Huo*[1], Xu Li[2a], Dongdong Chen[1] and Hongnan Li[1,3]

[1]*State Key Laboratory of Coastal and Offshore Engineering, Dalian University of Technology, No. 2 Linggong Road, Dalian 116024, China*
[2]*CITIC Construction CO., LTD, No. 2 East Third Ring Road, Beijing 100027, China*
[3]*School of Civil Engineering, Shenyang Jianzhu University, No. 9, Hunnan East Road, Shenyang 110168, China*

(Received July 25, 2017, Revised August 10, 2017, Accepted August 19, 2017)

Abstract. Piezoceramic transducers have been widely used in the health monitoring of civil structures. However, in most cases, they are used as sensors either to measure strain or receive stress waves. This paper proposes a method of using piezoelectric transducers as strain gauges and acoustic emission (AE) sensors simultaneously. The signals received by piezoceramic transducers are decomposed into different frequency components for various analysis purposes. The low-frequency signals are used to measure strain, whereas the high-frequency signals are used as acoustic emission signal associated with local damage. The b-value theory is used to process the AE signal in piezoceramic transducers. The proposed method was applied in the bending failure experiments of two reinforced concrete beams to verify its feasibility. The results showed that the extracted low-frequency signals from the piezoceramic transducers had good agreement with that from the strain gauge, and the processed high-frequency signal from piezoceramic transducers as AE could indicate the local damage to concrete. The experimental results verified the feasibly of structural health monitoring using piezoceramic transducers as strain gauges and AE sensors simultaneously, which can advance their application in civil engineering.

Keywords: piezoceramic transducer; strain gauge; acoustic emission; structural health monitoring; concrete structures

1. Introduction

The development and application of structural health monitoring (SHM) techniques in civil engineering have attracted great attention in recent years (Li *et al.* 2016). The use of the piezoelectric materials such as lead zirconate titanate (PZT) provides a much more efficient and convenient method of SHM owing to their dual functions of sensing and actuating (Li *et al.* 2014). Piezoelectric ceramic materials, which are characterized by their low cost, good electromechanical coupling properties and easy combination with structures by embedding or pasting, are appropriate for manufacturing as transducers with multiple functions (Song *et al.* 2007, 2008).

Piezoceramic is especially suited for strain sensing owing to its direct piezoelectric, which can convert stress or strain energy into electrical energy (Wang *et al.* 2016). The piezoelectric nanogenerator fabricated from zinc oxide (ZnO) nanowires inspired wide interest in piezoelectric nanomaterials and enabled new applications of strain sensing (Jenkins *et al.* 2015). Applications for strain sensing based on piezoelectric nanomaterials are numerous, including structural health monitoring, MEMS/NEMS devices, and human-computer interaction (Yang *et al.* 2009, Zhang *et al.* 2014).

Based on PZT, various kind of transducers were developed in recent years. Smart aggregates (SAs), which are fabricated by connecting a lead zirconate titanate (PZT) patch with wire, a waterproof covering and a protective layer, can monitor the inner stress and emit and receive the elastic wave that propagates in structures (Feng *et al.* 2016, Kong *et al.* 2014). Smart aggregates have been used to detect damage in reinforced-concrete beams (Song *et al.* 2007), columns (Gu *et al.* 2010), shear walls (Yan *et al.* 2009), frame structures (Laskar *et al.* 2009), fiber reinforced polymer (FRP) concrete columns (Howser *et al.* 2011) and bridges (An *et al.* 2014), the concrete freeze–thaw process (Kong *et al.* 2014), very-early-age concrete hydration (Kong *et al.* 2013) and debonding between the steel tube and confined concrete core of concrete-filled steel tubes (CFSTs) (Xu *et al.* 2013). An another PZT based sensor, smart washer, which combine with active sensing approach (Huo *et al.* 2017) and impedance method (Huo *et al.* 2017) can effective detect the bolt looseness. With the use of the Time Frequency Autoregressive Moving Average (TFARMA) model, a time domain impedance damage index based on Singular Value Decomposition (SVD) is defined to identify the damage in truss bridges (Fan *et al.* 2016).

Damage and deterioration in concrete can cause poor performance of structures under service loading. Hence, it is very important to understand the phenomena associated with cracking in order to give early warning and maintain the structure for both safety and economic considerations (Prem and Murthy 2017). The non-destructive evaluation of concrete structures has long been an engineering challenge

*Corresponding author, Associate Professor
E-mail: lshuo@dlut.edu.cn
[a]Ph.D.
E-mail: lx3818262@163.com

ISSN: 1598-8198 (Print), 1598-818X (Online)

and a popular research topic. Among various non-destructive evaluation techniques, acoustic emission (AE) has been attracting increasing attention because it is a promising tool for the long-term monitoring and evaluation of the damage evolution in concrete structures (Li *et al.* 2016). The AE technique has been used to monitoring the cracking, fatigue and damage of concrete structures (Li and Cao 2012, Li *et al.* 2012, Shahidan *et al.* 2017, Zhou *et al.* 2016). The advantages of the AE technique are that the locations of developing cracks can be determined, and the whole structure can be tested at once without intruding into any process associated with the structure (Colombo *et al.* 2003, Li *et al.* 2015). Conventionally, AE sensors are surface-mounted on the host structure. However, the AE signals attenuate quickly because of the high attenuation properties of concrete structures. To avoid the disadvantages of externally-mounted AE sensors, Li *et al.* (2016) proposed the method of using smart aggregates (SAs) as embedded AE sensors for the health monitoring of concrete structures.

In most cases of structural health monitoring, piezoceramic transducers are used as sensors either to measure strain or receive stress waves. This paper proposes a method of using piezoceramic transducers as strain gauges and AE sensors simultaneously, which is achieved by decomposing the signals they receive into various frequency components based on a wavelet algorithm. The low-frequency components are used to measure strain, whereas the high-frequency components are processed by the AE technique to evaluate the damage to the structure. The feasibility of the proposed method was verified in bending failure experiments on reinforced concrete beams.

2. Wavelet decomposition of signals based on the mallat algorithm

Piezoceramic transducers have a wide range of frequency responses, as a result the signals received by them in SHM are usually a combination of low-frequency signals related to structural response and high-frequency signals related to AEs caused by internal damage. The wavelet analysis technique provides an effective tool for the separation of signals in piezoceramic transducers for various functions. Compared with Fourier transform, the phase of reconstructed signal which decomposed by wavelet can be effective reduced. The information on phase is lost in the Fourier transform reconstructed signal. Hence, more real phase information is kept by wavelet decomposition. The Mallat algorithm for wavelet analysis is a fast algorithm with tower-type multi-resolution analysis and reconstruction (Mallat 1989), which can be described as follows: An important analytical scaling function $\phi(t)$ is introduced; The family functions $\{\phi_{j,n}(t)\}_{n\in Z}$ are acquired by stretching and translating the scaling function, which formed the orthogonal norm of the scale space V_j; The approximate signal $f_{Aj}(t)$, which is the orthogonal projection of signal $f(t)$ on V_j, can be expressed as an orthogonal expanded formula in $\{\psi_j,n(t)\}_{n\in Z}$, and the expansion coefficient $a_j(n)$ is the wavelet coefficient of the approximate part. Similarly, the functional group $\{\psi_j,n(t)\}_{n\in Z}$, which consisted of the orthogonal basis of the wavelet space W_j, can be obtained by stretching and translating the orthogonal wavelet function $\psi(t)$ (Ng 2014, Rizzo *et al.* 2004). The detail signal $f_{Dj}(t)$, which is the orthogonal projection $f(t)$ on W_j, can also be expressed as a form of orthogonal expansion, and the expansion coefficient $d_j(n)$ is the wavelet coefficient of the detail part. In the Mallat algorithm, the scale function and wavelet function are replaced by the digital filters $h(n)$ and $g(n)$. The $g(n)$ and $h(n)$ are shown as Eqs. (1) and (2)

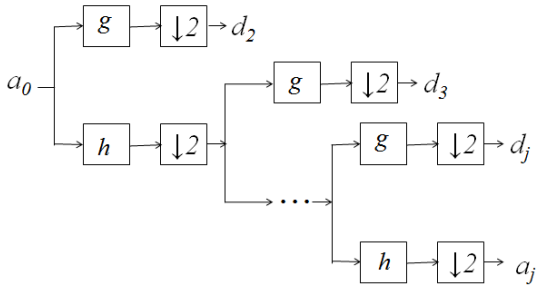

Fig. 1 The Mallat decomposition algorithm

$$h(n)=\sqrt{2}\int_{-\infty}^{+\infty}\phi(t)\phi(2t-n)dt \tag{1}$$

$$g(n)=\sqrt{2}\int_{-\infty}^{+\infty}\psi(t)\phi(2t-n)dt \tag{2}$$

The Mallat decomposition algorithm expressions are shown in Eqs. (3) and (4)

$$a_{j+1}(n)=\sum_k h(k-2n)a_j(k) \tag{3}$$

$$d_{j+1}(n)=\sum_k g(k-2n)a_j(k) \tag{4}$$

where h and g represent convolution manipulations, k=1,2,3,4…K, n is translation parameter in time axis respectively. In Eqs. (3) and (4), the wavelet coefficient a_{j+1} of the approximate portion for the signal $f(t)$ at a scale of 2^{j+1} (j+1th layer) is obtained in two steps: (1) Convolute the wavelet coefficient a_j of the approximate portion for the signal $f(t)$ at a scale of 2^j (jth layer) with the decomposition filter h; (2) Get the convolution results from a down-sampling that keeps one out of two. While the wavelet coefficient d_{j+1} of the detail portion for signal $f(t)$ at a scale of 2^{j+1}, which is also the high-frequency portion, is convoluted by the discrete approximation coefficient a_j at a scale of 2^j (jth layer) and decomposition filter g, then the convolution results are sampled point by point. The process of the Mallat decomposition algorithm is shown in Fig. 1.

Where h and g represent convolution manipulations; $\downarrow 2$ means a down-sampling that keeps one out of two.

The signals received by piezoelectric ceramic sensors consisted of two parts: the structural stress response caused by vibration and the acoustic emission signal caused by structural damage. The structural stress signals caused by structural vibration are generally low-frequency signals that range from zero to several hundred hertz, whereas the frequency of the acoustic emission signals is distributed in the high-frequencies, which range from several kilohertz to

several megahertz. Structural stress and acoustic emission signals have little overlap in the frequency range, which can be distinguished in the frequency domain. The selection of a compactly-supported orthogonal wavelet base decomposes the piezoelectric sensor signal $f_{pzt}(t)$ in the level j Mallat. The signal components S_V, which represent the structural dynamic characteristics, typically use the reconstruction signals of the approximate wavelet coefficients, which are decomposed by wavelet. The acoustic emission signal component S_A is the accumulation of the detail signal, and the formulas can be expressed by Eqs. (5) and (6)

$$S_V = f_{Aj}(t) \tag{5}$$

$$S_A = \sum_{i=1}^{j} f_{Di}(t) \tag{6}$$

where f_{Aj} represent the signal components that reflect structural vibration characteristics, f_{Dj} represent the AE signal.

3. "*b*-value" analysis of acoustic emission signals

The *b*-value theory was proposed in the field of seismology and gradually applied to the analysis of acoustic emissions (Colombo *et al.* 2003). The theory was based on the following facts: the amplitude is usually high for lower frequency AE events, whereas the amplitudes of high-frequency acoustic emission events are very low. Therefore, by calculating the slope of the amplitude distribution, the *b*-values can be used to determine the amplitude distribution of AE events (Colombo *et al.* 2003). The *b*-value is given by Eq. (7)

$$\log_{10} M = a - b(A_{dB}/20) \tag{7}$$

where b is b value, A_{dB} is the amplitude of AE signal, M is the cumulative number of AE events whose peak amplitude (dB) is greater than the A_{dB}, a is a constant and the *b*-value indicates the distribution slope of AE events with different amplitudes.

The essence of the *b*-value is the amplitude statistics of AE, which reflect the cracking status of the structure (Carpinteri *et al.* 2008). The decrease in the *b*-value indicates a process change from microcrack to macrocrack, and the change in the *b*-value captures the process of crack formation and development.

In the *b*-value theory analysis, a and b are time history parameters. Therefore, the damage status of the structure can be represented as the growth speed of AE events at a certain level. Eq. (7) is re-expressed by A_0, whose unit is voltage, and an acoustic emission accumulated time parameter β_t is introduced as follows (Carpinteri *et al.* 2008)

$$N(\geq A_0, t) = 10^{a(t)} A_0^{-b(t)} = t^{\beta_t} \tag{8}$$

where A_0 is the AE signal amplitude with certain level. $N(\geq A_0, t)$ is the cumulative number of AE events whose amplitudes are greater than or equal to A_0. β_t reflect the speed of damage development. As show in Fig. 2 (Carpinteri *et al.* 2008), β_t=1 is a damage threshold: when the β_t<1, the development speed of N is very slow. When β_t>1, N has sharp growth, which means that the structural damage is serious and there is a loss of bearing capacity and the structure might even be about to collapse.

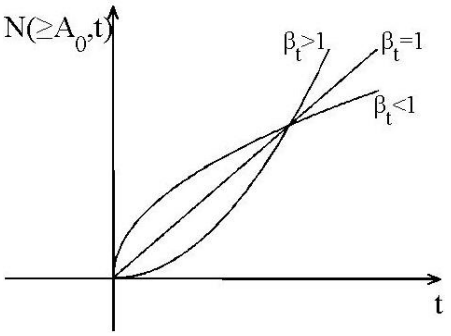

Fig. 2 Illustration of β_t with three conditions

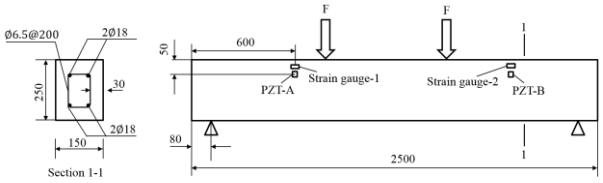

Fig. 3 Experimental setup

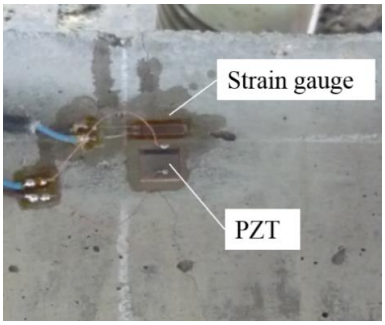

Fig. 4 Photo of PZT sensor and strain sensor

4. Experimental study

4.1 Introduction of the experiment

In this section, taking the dynamic bending failure test of reinforced concrete as an example, the multifunctional application of piezoelectric ceramic sensors in the monitoring of concrete component failure is described. The size and reinforcement of a beam are shown in Fig. 3. The concrete strength is C30. The longitudinal reinforcements are HRB335 steel, reinforced at a diameter of 18 mm. The stirrups are HPB235 steel with a diameter of 6.5 mm and a spacing of 200 mm throughout the layout. The reinforcement ratio of the longitudinal reinforcements was 1.4%, and the reinforcement ratio of stirrups was 0.22%. The largest size of the coarse aggregates is only 10 mm, which is very small compared with the one of the beam, so the influence of aggregate can be neglected for the proposed

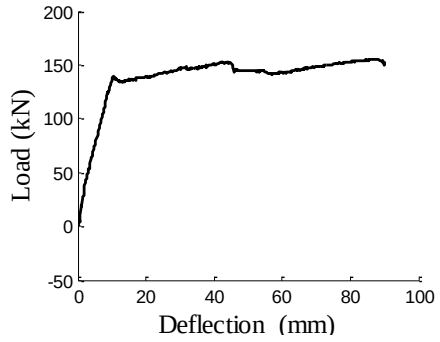

(a) Test specimen 1

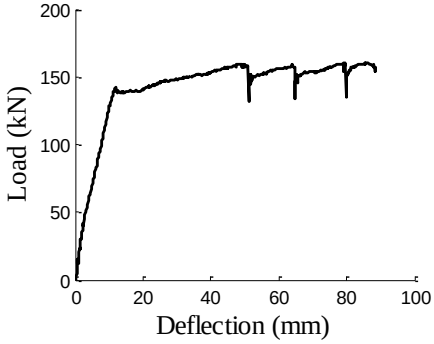

(b) Test specimen 2

Fig. 5 Load-displacement curve

method.

Two adhesive PZT sensors are arranged at a distance of 600 mm from each beam end and 50 mm from the upper edge of the specimen. A strain sensor is arranged near each of the PZT sensors. These sensors are shown in Fig. 4. The thickness of each PZT is 1 mm, and its size is 10 mm×10 mm. The small size of the PZT transducer will be more sensitive to accept the AE signal. To get a tradeoff between the sensitivity and convenience of PZT pasting, this size of PZT sensors are selected as 10 mm×10 mm×1 mm. The location of a pasted PZT is shown in Fig. 3. The PZT signal was sampled with a PXI virtual instrument at a sampling rate of 200 kHz. A 2500-kN concrete dynamic triaxial testing machine with a loading rate of 30 mm/s was employed. Two sets of test specimens (1 and 2) were used and the load-deflection curve is shown in Fig. 5. There are discreteness exits in the concrete experiment. The creaks could not happen in the same zone for different specimens even in same type. Hence, the loading curves are also different with each other.

4.2 Acoustic emission component of PZT sensor signal

The collected PZT signal is shown in Fig. 6. This signal contains both the strain response component of the concrete beam and the fracture-caused acoustic emission component. By using the 'db25' wavelet base, the sensor signal is decomposed and reconstructed into five wavelet levels. As shown in Eq. (6), the approximation signal is a low-frequency structural strain response signal, and the acoustic emission signal, which was released by the structural failure, was accumulated by the detail signal.

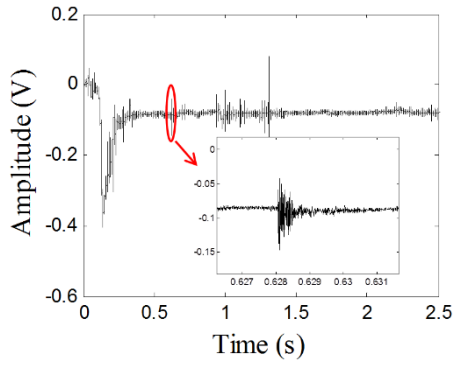

(a) Sensor A of specimen 1

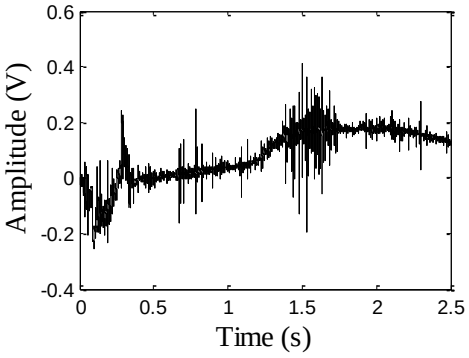

(b) Sensor B of specimen 1

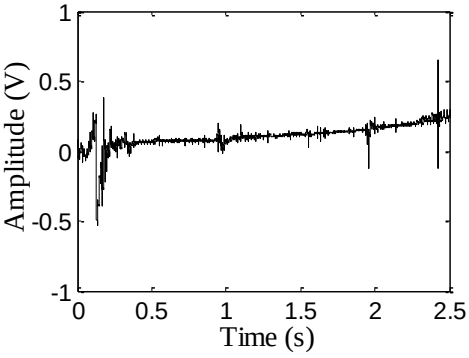

(c) Sensor A of specimen 2

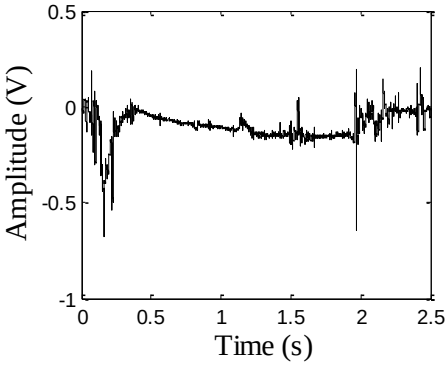

(d) Sensor A of specimen 2

Fig. 6 PZT sensor signals

The waveform comparison between the low-frequency voltage signal of the PZT sensor on test specimen 1 and the strain signal from test specimen 2 is shown in Figs. 7 and 8, respectively. It can be seen that the waveform of PZT sensor is similar to the waveform of the resistance strain sensor; they are only somewhat different in Fig. 7(a). Fig. 7(a)

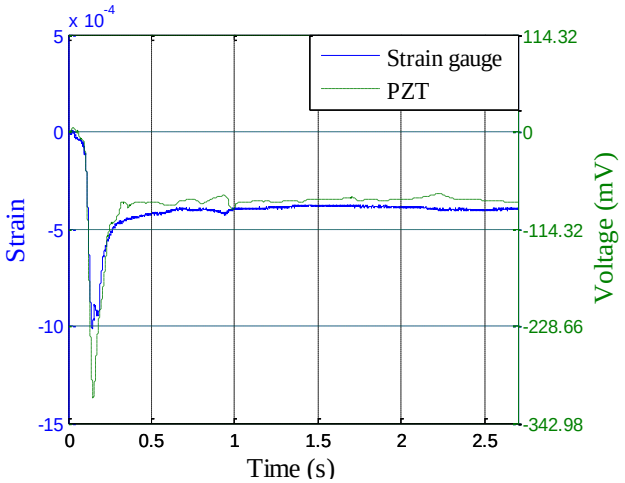

(a) PZT sensor A and strain sensor 1

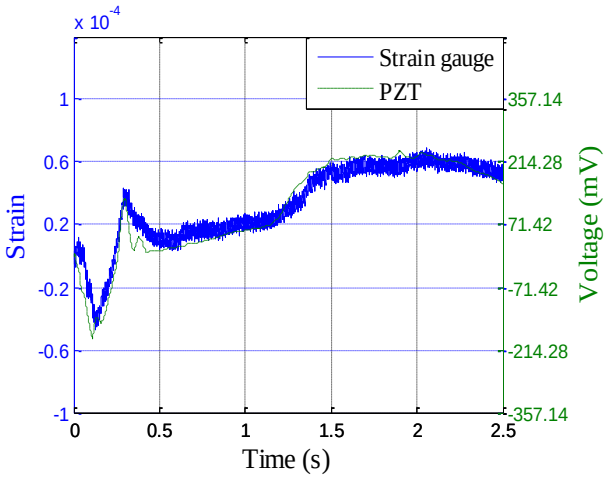

(b) PZT sensor B and strain sensor 2

Fig. 7 Voltage signal from PZT sensor and strain signal from strain sensor on specimen 1

shows that the amplitude of the strain signal is in the range of 0 to 13×10^{-4}, which is much larger than the amplitude range of the other strain signals. It should be notice that the ordinate range in Fig. 7(a) is different with Fig. 7(b), and Figs. 8(a) and 8(b), all those signals are in same noise level. The waveform difference between the two sensor signals may be caused by an abnormality of the strain sensor in test specimen 1(a). The different coordinate scale in these figures is to illustrate the coordinate of two plotted signal and demonstrate the feasibility of using piezoceramic transducers as strain gauges and AE sensors to monitor the healthy state of structure. Therefore, the strain response component extracted from the piezoelectric ceramic sensor can reflect the structural strain change effectively.

4.3 Structural strain response in PZT sensor signal

The flexural failure process of reinforced the concrete beam can be divided into three stages. As shown in Fig. 9, the relationship between deflection and load is linear in the first phase, and the major acoustic emission source of the concrete is microcracks, which gradually formed and expanded in the bottom of beam. In the second stage, the

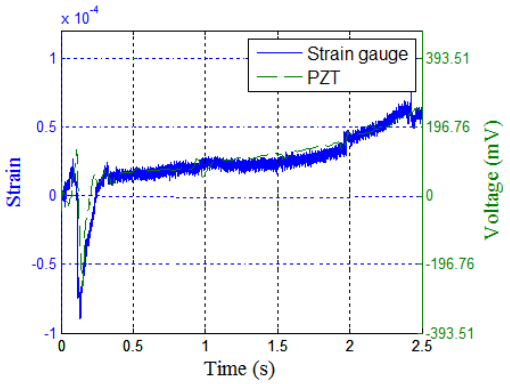

(a) PZT sensor A and strain sensor 1

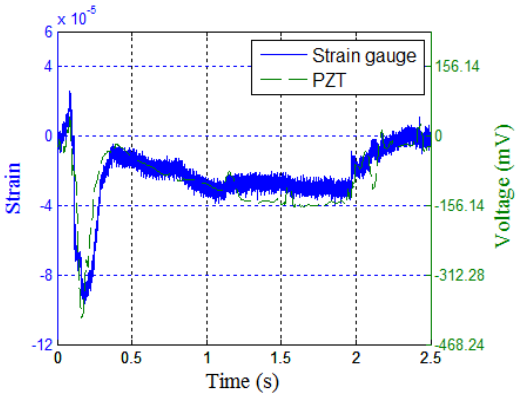

(b) PZT sensor B and strain sensor 2

Fig. 8 Voltage signal from PZT sensor and strain signal from strain sensor on specimen 2

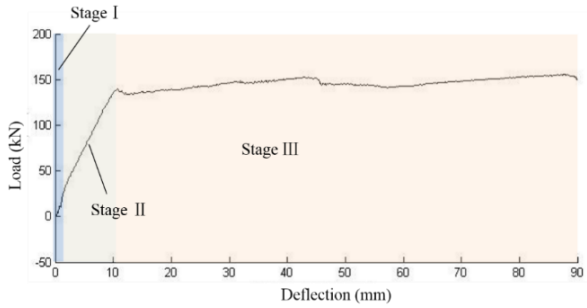

Fig. 9 Three stages of the reinforced concrete beam bending failure

macroscopic cracks, which were located in the bottom of the beam, began to expand and generate AE events. In the third phase, the tension reinforcement yield and compressed concrete reach the ultimate compressive strength and are then damaged. The major acoustic emission source is caused by instability between the steel rebar and concrete. The reason why there are differences among the acoustic emission waveform signal characteristics is that the formation mechanisms of the acoustic emission source in the three stages of reinforced concrete beam flexural failure are not the same.

The overall waveform acoustic emission signal can provide more comprehensive and detailed acoustic emission signal characteristic information. The acoustic emission signal waveform of piezoelectric sensors in the range 10 to 100 kHz was shown in Fig. 10, in which (a)-(e) represent

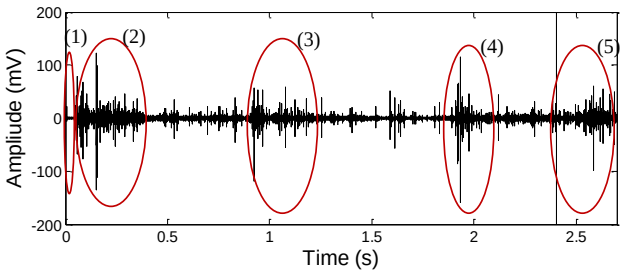

Fig. 10 AE signal from PZT sensor

several higher energy waveform with active AE than other data. Section (1) is the first phase of the acoustic emission signal with a length of 10,000 data points. Section (2) is the second phase of the acoustic emission signal. Section (3), (4) and (5) represented the higher energy acoustic emission signal in the third phase with the length of 60,000 data points. Compared with other period of signal, the length of section (1) is relatively short, so the influence of the length of the acoustic emission signal on the spectrum characteristic was first analysed.

The analysis of the signal power spectral density in periods of Sections (1)-(5) is shown in Fig. 11. It can be seen that the peaks of the signal spectrum diagram are mainly concentrated in the range of 20-40 kHz. In the signal spectrum diagram of section (2), large amplitude frequency points are mainly concentrated at 40 and 51.17 kHz. In section (3), the frequency points at 40, 51.17 and 52.27 kHz have large amplitudes. In section (4), larger amplitude frequency points are located at 40, 52.27, 54, 66.8 and 70 kHz. In the signal period of (5), spectrum peaks are mainly concentrated in the range of 48 to 72 kHz. In the damage process, the trend of the acoustic emission signal spectrum frequency peaks gradually increases. As the damage develops, the peaking frequency points of the acoustic emission wave rise as well. Therefore, by analysing the spectrum of the acoustic emission signal, the degree of damage of the reinforced concrete beam can be further estimated.

The acoustic emission events are extracted from the whole-time history, and the amplitude information of each AE event is counted. The method of extracting the acoustic emission event is as follows: First, set a threshold voltage; then, intercept the acoustic emission signal when the envelope exceeds the threshold voltage, as shown in Fig. 12. The threshold voltage should be higher than the background noise and lower than the AE signal. In this section, the threshold voltage is 5 mV, and the data length of the acoustic emission signal is 200 points.

The amplitude distribution of the acoustic emission events extracted from the signal of sensors in test specimens 1 and 2 are shown in Fig. 13. It can be seen that the amplitude distribution of the acoustic emission event satisfies the linear relationship described by the *b*-value theory. The amplitude of the acoustic emission signal obtained by the PZT sensor can reflect the amplitude of the actual acoustic emission stress wave.

The distribution of the amplitude of the acoustic emission event by time is analyzed in the damage process. Fig. 14 shows the amplitude distribution of the acoustic

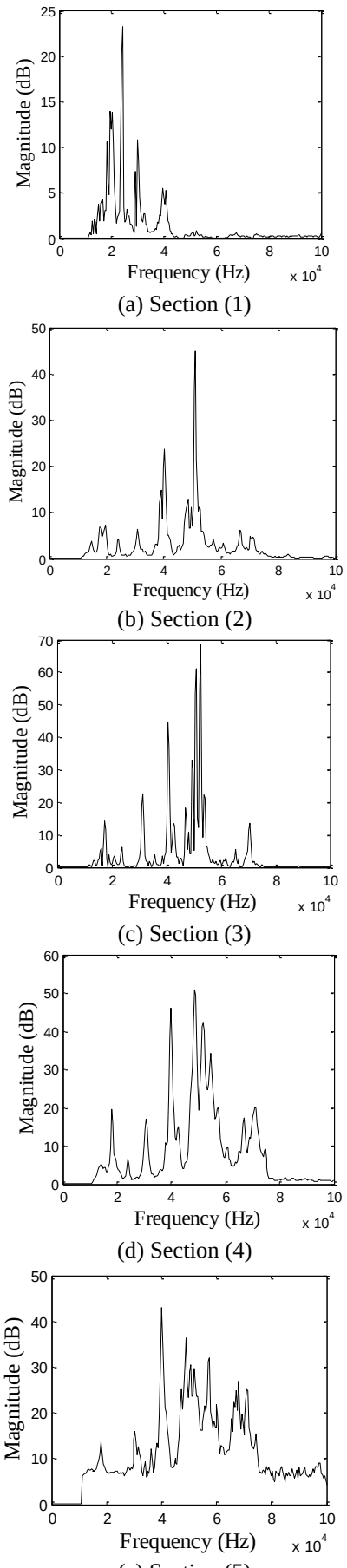

(a) Section (1)

(b) Section (2)

(c) Section (3)

(d) Section (4)

(e) Section (5)

Fig. 11 AE signal from PZT sensor

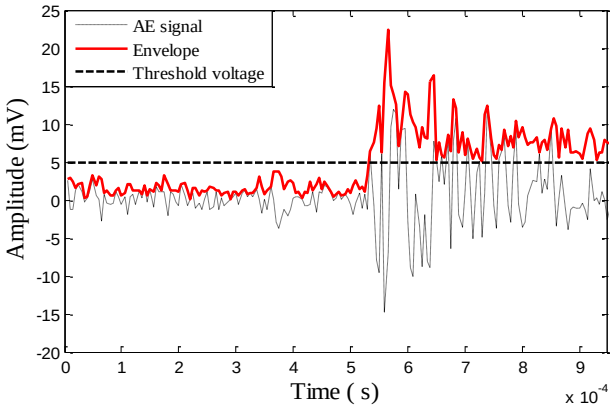

Fig. 12 Diagram of an AE event signal

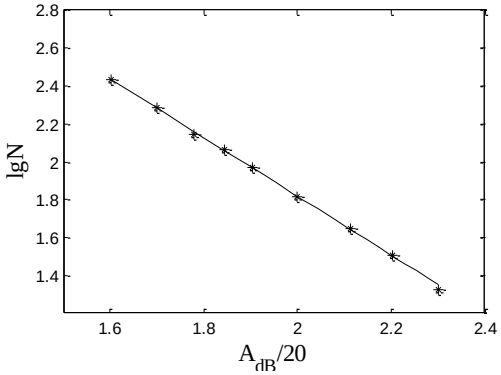

(a) Specimen 1

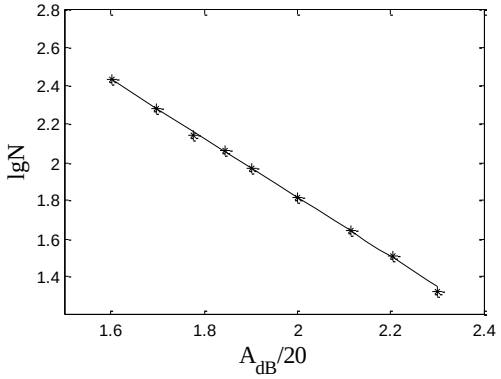

(b) Specimen 2

Fig. 13 AE amplitude distribution

emission event by time is analyzed in the damage process. Fig. 14 shows the amplitude distribution of the acoustic emission event for sensor B in test specimen 2, and the frequency of acoustic emission event in Fig. 14(a) is in the range of 10 to 100 kHz. It can be seen that the energy of the acoustic emission event in phase I is much smaller, but the quality and amplitude of acoustic emission events are significantly improved in stages II and III. Fig. 14(b) is the acoustic emission event distribution below 10 kHz, typically in the range of 1 to 5 kHz. It can be seen that the amplitude of the acoustic emission event is much larger and most of them concentrated in the second stage, which means that this is a macroscopic cracking stage. To a certain extent, the acoustic emission signal in this frequency range reflects the macroscopic cracking of concrete.

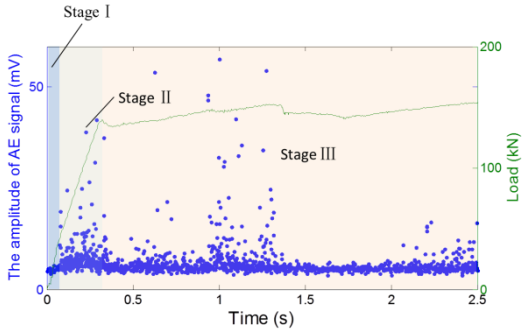

(a) Distribution of AE amplitudes between 10-100

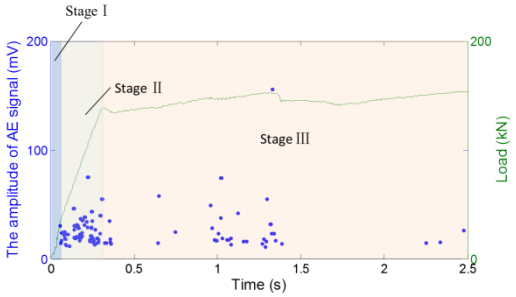

(b) Distribution of AE amplitudes below 10 kHz

Fig. 14 AE amplitude distribution

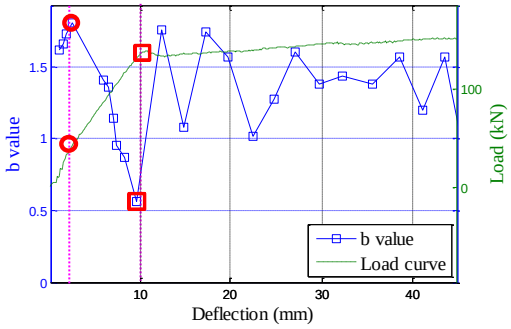

(a) Specimen 1

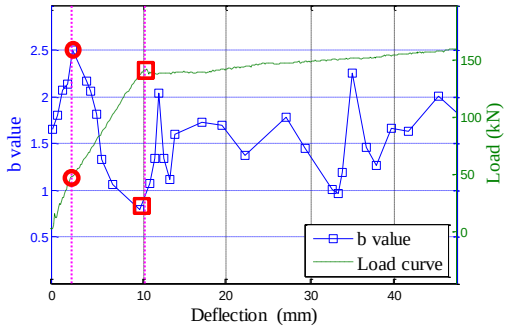

(b) Specimen 2

Fig. 15 B-values and loading curves

Seventy acoustic emission events were taken as a group and the *b*-value of the acoustic emission events in each group was calculated. Fig. 15 shows the load deflection curves for the test specimens of 6-1 and 6-2, and the corresponding change in *b*-value calculated by the sensor A varies with deflection. When the deflection is up to 2.58 mm (marked by circles), the *b*-value begins to decrease. Because the first low *b*-value peak can be used to estimate

the occurrence of macro creaks and the plastic stage develop. It shows that the cracking status of the concrete beam has developed from micro to macrocracks. Moreover, it can be seen from the load-deflection curve that when the deflection is increased to 2.58 mm, the bearing capacity of the structure begins to gradually decrease because of the macroscopic cracking in the concrete, and the beam enters into the elastic-plastic stage. When the deflection increases to 10 mm (marked by boxes), the b-values are lowest, which indicates that the larger amplitude of the acoustic emission events takes the largest proportion, and the macroscopic fracture phenomenon of concrete at this point is the worst. The load-deflection curve can also indicate that the fracture surface of the beam is gradually formed and the beam begins to enter the yield stage. Therefore, the decline in the b-value indicates the beginning of macroscopic fracture, and the *b*-value analysis can be a warning approach for local damage to the concrete structure. Therefore, by emitting the acoustic emission signal through PZT sensors, an effective warning of local damage to the concrete beam can be provided.

Therefore, the low-frequency response signal of sensors can be applied to analyse the strain status of structures. In addition, the acoustic emission components of the sensor signal can be used to monitor the local damage of structures by applying the broadband response of the piezoelectric ceramic sensor, the strain response and local damage of the structure can be monitored simultaneously.

5. Conclusions

In this paper, a method of using piezoceramic transducers as strain gauges and AE sensors simultaneously was proposed and experimentally investigated. The Mallat wavelet algorithm was used to decompose the signals in piezoceramic transducers into different frequency ranges. The low-frequency signal was used to measure strain, and the high-frequency signal was used to process the *b*-value analysis of the AE. The results showed that the extracted low-frequency signals from piezoceramic transducers had good agreement with those from strain gauges, and the processed high-frequency signals from piezoceramic transducers as AE could indicate the local damage in concrete. The results confirmed the feasibility of using piezoceramic transducers as strain gauges and AE sensors for the health monitoring of concrete structures. Although the results from the laboratory tests are encouraging, the efficacy of the proposed method has never been tested in practical applications. In the future, a further feasibility study on practical applications of the proposed method will be conducted.

Acknowledgments

This research was partially supported by the Major State Basic Development Program of China (973 Program, grant number 2015CB057704), Innovative research group project (grant number 51421064) and general project (grant numbers 51478080) of Natural Science Foundation of China, and the Fundamental Research Funds for the Central Universities (DUT16TD03). The authors would like to acknowledge these organizations for their financial support.

References

An, Y.K., Lim, H.J., Kim, M.K., Yang, J.Y., Sohn, H. and Lee, C.G. (2014), "Application of local reference-free damage detection techniques to in situ bridges", *J. Struct. Eng.*, **140**(3), 04013069.

Carpinteri, A., Lacidogna, G., Niccolini, G. and Puzzi, S. (2008), "Critical defect size distributions in concrete structures detected by the acoustic emission technique", *Meccan.*, **43**(3), 349-363.

Colombo, I.S., Main, I.G. and Forde, M.C. (2003), "Assessing damage of reinforced concrete beam using "b-value" analysis of acoustic emission signals", *J. Mater. Civil Eng.*, **15**(3), 280-286.

Fan, X., Li, J. and Hao, H. (2016), "Piezoelectric impedance based damage detection in truss bridges based on time frequency ARMA model", *Smart Struct. Syst.*, **18**(3), 501-523.

Feng, Q., Kong, Q.Z. and Song, G.B. (2016), "Damage detection of concrete piles subject to typical damage types based on stress wave measurement using embedded smart aggregates transducers", *Measure.*, **88**, 345-352.

Gu, H.C., Moslehy, Y., Sanders, D., Song, G.B. and Mo, Y.L. (2010), "Multi-functional smart aggregate-based structural health monitoring of circular reinforced concrete columns subjected to seismic excitations", *Smart Mater. Struct.*, **19**(6), 065026.

Howser, R., Moslehy, Y., Gu, H.C., Dhonde, H., Mo, Y.L., Ayoub, A. and Song, G.B. (2011), "Smart-aggregate-based damage detection of fiber-reinforced-polymer-strengthened columns under reversed cyclic loading", *Smart Mater. Struct.*, **20**(7), 075014.

Huo, L., Chen, D., Kong, Q., Li, H.N. and Song, G.B. (2017), "Smart washer-a piezoceramic-based transducer to monitor looseness of bolted connection", *Smart Mater. Struct.*, **26**(2), 025033.

Huo, L., Chen, D., Liang, Y.B., Li, H.N., Feng, X. and Song, G.B. (2017), "Impedance based bolt pre-load monitoring using piezoceramic smart washer", *Smart Mater. Struct.*, **26**(5), 057004.

Jenkins, K., Nguyen, V., Zhu, R. and Yang, R.S. (2015), "Piezotronic effect: An emerging mechanism for sensing applications", *Sens.*, **15**(9), 22914-22940.

Kong, Q.Z., Hou, S., Ji, Q., Mo, Y.L. and Song, G.B. (2013), "Very early age concrete hydration characterization monitoring using piezoceramic based smart aggregates", *Smart Mater. Struct.*, **22**(8), 085025.

Kong, Q.Z., Wang, R.L., Song, G.B., Yang, Z.H. and Still, B. (2014), "Monitoring the soil freeze-thaw process using piezoceramic-based smart aggregate", *J. Cold Reg. Eng.*, **28**(2), 06014001.

Laskar, A., Gu, H., Mo, Y.L. and Song, G. (2009), "Progressive collapse of a two-story reinforced concrete frame with embedded smart aggregates", *Smart Mater. Struct.*, **18**(7), 075001.

Li, D.S. and Cao, H. (2012), "Monitoring of temperature fatigue failure mechanism for polyvinyl alcohol fiber concrete using acoustic emission sensors", *Sens.*, **12**(7), 9502-9513.

Li, D.S., Chen, Z., Feng, Q.M. and Wang, Y.L. (2015), "Damage analysis of CFRP-confined circular concrete-filled steel tubular columns by acoustic emission techniques", *Smart Mater. Struct.*, **24**(8), 085017.

Li, D.S., Hu, Q. and Ou, J.P. (2012), "Fatigue damage evolution and monitoring of carbon fiber reinforced polymer bridge cable by acoustic emission technique", *J. Distrib. Sens. Netw.*, 282139.

Li, H., Yi, T., Ren, L., Li, D. and Huo, L. (2014), "Reviews on

innovations and applications in structural health monitoring for infrastructures", *Struct. Monitor. Mainten.*, **1**(1), 1-45.
Li, J. and Hao, H. (2016), "A review of recent research advances on structural health monitoring in Western Australia", *Struct. Monitor. Mainten.*, **3**(1), 33-49.
Li, W.J., Kong, Q.Z., Ho, S.C.M., Lim, I., Mo, Y.L. and Song, G.B. (2016), "Feasibility study of using smart aggregates as embedded acoustic emission sensors for health monitoring of concrete structures", *Smart Mater. Struct.*, **25**(11), 115031.
Mallat, S.G. (1989), "A theory for multiresolution signal decomposition-the wavelet representation", *IEEE Trans. Patt. Analy. Mach. Intell.*, **11**(7), 674-693.
Ng, C.T. (2014), "On the selection of advanced signal processing techniques for guided wave damage identification using a statistical approach", *Eng. Struct.*, **67**, 50-60.
Prem, P.R. and Murthy, A.R. (2017), "Acoustic emission monitoring of reinforced concrete beams subjected to four-point-bending", *Appl. Acoust.*, **117**, 28-38.
Rizzo, P. and Lanza Di Scalea, F. (2004), "Discrete wavelet transform to improve guided-wave-based health monitoring of tendons and cables", *SPIE Proc.*, **5391**, 523-532.
Shahidan, S., Pullin, R., Bunnori, N.M. and Zuki, S.S.M. (2017), "Active crack evaluation in concrete beams using statistical analysis of acoustic emission data", *Insight*, **59**(1), 24-31.
Song, G.B., Gu, H.C. and Mo, Y.L. (2008), "Smart aggregates: Multi-functional sensors for concrete structures-a tutorial and a review", *Smart Mater. Struct.*, **17**(3), 033001.
Song, G., Gu, H., Mo, Y.L., Hsu, T.T.C. and Dhonde, H. (2007), "Concrete structural health monitoring using embedded piezoceramic transducers", *Smart Mater. Struct.*, **16**(4), 959-968.
Wang, J.J., Kong, Q.Z., Shi, Z.F. and Song, G.B. (2016), "Electromechanical properties of smart aggregate: Theoretical modeling and experimental validation", *Smart Mater. Struct.*, **25**(9), 095008.
Xu, B., Li, B. and Song, G.B. (2013), "Active debonding detection for large rectangular CFSTs based on wavelet packet energy spectrum with piezoceramics", *J. Struct. Eng.*, **139**(9), 1435-1443.
Yan, S., Sun, W., Song, G.B., Gu, H.C., Huo, L.S., Liu, B. and Zhang, Y.G. (2009), "Health monitoring of reinforced concrete shear walls using smart aggregates", *Smart Mater. Struct.*, **18**(4), 047001.
Yang, Y., Qi, J.J., Gu, Y.S., Wang, X.Q. and Zhang, Y. (2009), "Piezotronic strain sensor based on single bridged ZnO wires", *Phys. Stat. Sol.-Rap. Res. Lett.*, **3**(7-8), 269-271.
Zhang, W.G., Zhu, R., Nguyen, V. and Yang, R.S. (2014), "Highly sensitive and flexible strain sensors based on vertical zinc oxide nanowire arrays", *Sens. Actuat.-Phys.*, **205**, 164-169.
Zhou, X., Yang, Y.Y., Li, X.Q. and Zhao, G.Q. (2016), "Acoustic emission characterization of the fracture process in steel fiber reinforced concrete", *Comput. Concrete*, **18**(4), 923-936.

HK